Heliyon 10 (2024) e26935

Contents lists available at ScienceDirect

Heliyon

journal homepage: www.cell.com/heliyon

Research article

Evaluation of LVRT capability and stability analysis of VSC based advanced control approach for grid connected PV system under grid fault conditions

Hussin Zahloul [a,b,*], Arjmand Khaliq [a,c], Hamed Hamzehbahmani [a], Sergii Veremieiev [a], Sana Salous [a]

[a] Department of Engineering, Durham University, DH1 3LE, Durham, United Kingdom
[b] Electrical Engineering Department, High Institute of Science and Technology, Tiji, Libya
[c] Architectural Engineering and Design Department, University of Engineering and Technology Lahore, Lahore, Pakistan

ARTICLE INFO

Keywords:
Grid connected PV system
Short circuit faults
VSC control
Voltage stability
Low voltage ride through (LVRT)

ABSTRACT

Short circuit faults are a prevalent issue in power systems, causing disruptions to the grid's normal operation. Dynamic behaviours of the conventional power systems during short circuit faults have been extensively studied and understood. The bulk of ongoing research and development are focusing on the dynamic performance of grid-connected renewable energy systems under these fault conditions, due to changes in the grid code and a decrease in system inertia. The development of effective control strategies to enhance the system's reliability during fault conditions is of paramount importance. In this paper, a two-stages grid-connected photovoltaic system (GCPV) having a rated power of 2 MW was created in the MATLAB/Simulink environment. The dynamic behaviour of the presented system was evaluated in two scenarios: steady state conditions and short circuit faults. A line-to-ground short circuit fault was created at the grid side, and its effect on the PV system's operation was observed. An advanced control system was designed to maintain stability during fault conditions. The results demonstrated the efficiency of the designated control system in minimizing the effects of short circuit faults on the GCPV system's function, and restoring the system promptly after the fault was cleared. Furthermore, considering modifications in grid regulations, the low voltage ride through (LVRT) capability of the designed system was analysed and validated according to the UK standards. The Total Harmonic Distortion (THD) level at the common coupling point was also analysed for voltage and current, remaining below the acceptable level of 5% as specified in the IEEE Std. 519.

1. Introduction

RENEWABLE energy resources have drawn great attention around the world due to the increased energy demand and concerns about climate change and global warming. As a result, a rapid increase in energy generation from renewable energy resources have been observed in the past few decades. Among all renewable resources, photovoltaic (PV) systems dominated other resources due to its advantages of easy installation, simple operation, and low maintenance cost [1,2]. Consistent with the International Renewable Energy

* Corresponding author. Department of Engineering, Durham University, DH1 3LE, Durham, United Kingdom.
E-mail address: hussin.a.zahloul@durham.ac.uk (H. Zahloul).

https://doi.org/10.1016/j.heliyon.2024.e26935
Received 12 September 2023; Received in revised form 19 February 2024; Accepted 21 February 2024
Available online 23 February 2024
2405-8440/

Agency (IREA) it is expected that by 2050, 15 % of the whole renewable energy of the world would be from solar PV systems [3,4].

Solar Power generators are mainly characterised based on operation into two categories: grid connected, and standalone systems [5]. Grid Connected Photovoltaic Systems (GCPV) are more common because of their advantages over the standalone systems. With the GCPV, energy is delivered to the grid according to the load demand. Furthermore, in GCPV systems there is no need for energy storage or back up system, which reduce the overall cost. It also increases the system's total efficiency by reducing the power losses caused by the energy storage units [6]. Due to the numerous features of the PV systems, it is expected that they will play a key role in Net-Zero economy [7]. However, to guarantee a stability and reliability as well as secure operation of the system an in-depth analysis on the integration criteria to the utility grid is required [8,9]. This is a one of the fundamental factors in the improved design and successful control of GCPV systems to prevent unfavourable consequences including voltage fluctuations, harmonics emission at the Common Coupling Point (CCP) and instability to the grid [10].

Connecting the renewable energy resources with power grid supports the operation of grid in meeting the growing energy demand though the increased ratio of these resources arises the concerns about its stable operation. With the changing scenarios by the addition of these renewable energy resources, power grid operators are continuously focusing and revising the grid codes and standards which can support the system according to new requirements. One of the most frequent conditions in such system is occurrence of grid faults and its impact on connected RE systems. For this condition, Low Voltage Ride Through (LVRT) regulations are devised for monitoring of system's stability under fault conditions [11]. LVRT is a condition during which all Renewable Energy Systems (RESs) must continue operating for a specified period to guarantee that the occurred fault is transient [12]. In other word, LVRT is ability of the RESs to remain in service during a voltage dip caused by a fault [13].

Before RES power plants can be integrated into the power grid, several tests must be conducted to evaluate their compatibility with the grid. These tests typically involve examining voltage and current fluctuations, power quality, LVRT capability, high-voltage ride through (HVRT) capability, reactive power compensation, and safety while operating in anti-islanding mode. These tests aim to assess whether the RES farms can function in compliance with the grid standards [11].

In the past LVRT requirements were mainly applied to wind turbines. This was because occurrence of three-phase fault on a transmission line could cause a complete loss of voltage at the fault point until the fault is cleared, resulting in a loss of power generation. However, with the increasing development of integrated solar power plants, there is a need to consider LVRT requirements for solar plants as well [11,12]. This is because when any disturbances or faults occur, complete interruption of power delivered by the solar farm can be unreliable and may lead to blackouts. Hence, it is recommended to validate LVRT capability before integrating RES with the grid. LVRT capability is generally evaluated for PV systems in the laboratory via LVRT test units [11]. In grid integrated renewable energy resources, LVRT capability is evaluated to keep converter connected with the grid during temporary fault as well as for transient stability and smooth resynchronisation when fault is cleared [14].

Performance of the GCPV systems including Maximum Power-Point Tracking (MPPT) [15,16], harmonic emission [17], power quality aspects [18,19], islanding detection techniques [17], and new fault detection approach in grid connected PV system [20] an adaptive FRT capability of virtual synchronous machine control for grid forming converter [21], have been investigated by other researchers. Like most of the other renewable energy systems, in a GCPV system the PV system is integrated to the utility grid using a power electronic converter with optimized control strategy, which controls the dynamic response and stability under various conditions including normal and abnormal operation. Optimized design of the power electronic converters and associated control strategies are crucially important to maintain a reliable implementation of the system, during steady-state and transient fault conditions. With the ever-increased demand of renewable energy systems, power system authorities are more concerned about providing efficient techniques to maintain stability of the grids during abnormal operations [22]. This requires improved control approaches for the power electronic converters.

Due to the operating characteristics of the PV arrays and the controlled operation of the inverter, solar PV systems inject low magnitude fault currents to the grid as compared to the conventional generator [23]. For the GCPV systems, in addition to the contribution of short circuit current by the PV systems, it is crucial to analyse effects of the grid fault on the function of the PV systems. The significantly increased addition of these systems and modifications in the grid codes by regulating authorities have encouraged the researchers to evaluate the impacts of abnormal grid conditions on the various parameters of the PV systems. Moreover, key requirement for successful delivery of power from the PV systems includes various components like power electronic converters, harmonic filters, and power transformers. If the function of these components is affected due to abnormal conditions, it may cause severe disturbances in power delivery. Therefore, it is substantially important to design and evaluate a control system which can work efficiently to minimize the impacts of grid abnormalities and maintain the power system stability during and after abnormal conditions.

Short circuit faults in power systems are caused by several abnormal conditions and depend on the parameters and configurations of the grid, they can inject transient fault currents of very high magnitude as compared to the rated load currents. Fault currents causes electrodynamic disruption and significant thermal losses on power system elements, that can result sever damages [24,25]. Short circuit faults are categorized to different types, amongst which line-to-ground (LG) faults are the most frequent, with a probability of 70–80 % [26,27].

During these fault conditions the operation of GCPV is supported by the integrated ancillary services. As LVRT capability curves are used for assessment of GCPV system's response under grid faults. Several techniques are applied to improve the LVRT response by using additional components like energy storage systems including batteries and capacitors, fault current limiters and static synchronous compensator (STATCOM). Though, addition of these hardware components will not only increase the overall cost and complexity of the system but will also become more challenging with the set goals of addition of high percentage of PV system in future. Recently the focus on these grid codes and compulsions by authorities have increased the importance of exploring advanced

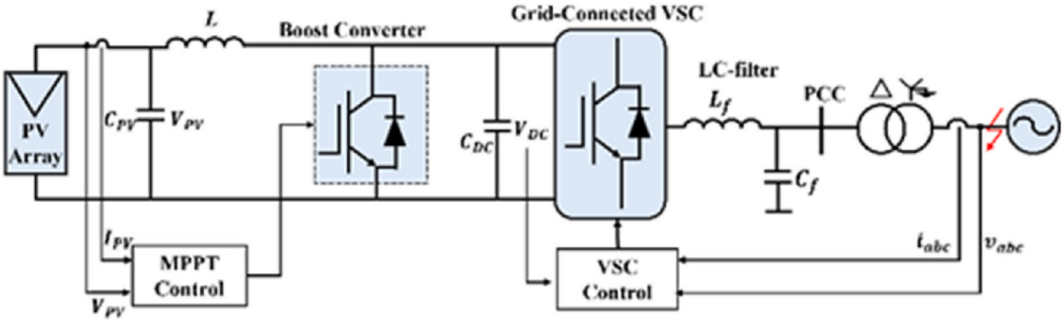

Fig. 1. Schematic of a GCPV system.

control schemes, depending upon the converter types and grid codes, which can support GCPVs during grid abnormalities [28]. In absence of a proper control scheme, it is recommended to either disconnect the PV system from the utility, or to change the PV arrays operating point on the characteristics curve to reduce the output power during fault conditions [29].

With the continuous increase of PV system in grids, increasing the converters' operating ratings have drawn great attention of researchers. In this paper, the generation capacity of the system has been increased using the VSC control scheme and system parameters are configured to evaluate stability under grid faults. One of the key objectives is to evaluate if VSC based control strategies can be implemented for large generation capacity of PV systems while maintaining the reliable dynamic response of the system. The dynamic response of the system is highly influenced by the sudden faults conditions. So, monitoring LVRT capability for evaluation of system's dynamic response under grid faults is crucial. The design of efficient control for dc link voltage and inverter operation is essential for successful LVRT operation. The control strategy is modified to minimize the impacts of grid faults on the DC link voltage which supports the dynamic operation of the PV systems during such abnormal condition [30]. In addition, it also maintains the stability of the overall system.

In [30] detailed review has been conducted for evaluation of various inverter control methods and it was recommended that advanced control approaches should be encouraged as addition of additional hardware support will increase the cost and complexity of the system. The comparative analysis of various techniques and grid codes has been performed but generation capacity of the system has not been considered which is major factor for designing the various components of the overall system as well as stable dynamic operation.

In [31] novel control scheme is analytically applied for a single stage system with large capacity of 1.5 MW and LVRT capability was improved but presented results do not provide information about the grid codes or standards. Moreover, it is equally crucial to evaluate the LVRT capability for double stage grid connected PV systems for improving the LVRT as the ratio of addition of these systems is continuously increasing because of the set goals of net zero in near future.

In [32] an appropriate charging and discharging algorithm for the battery energy storage was presented for mitigation of over voltages caused by connected PV systems. However, voltage sags are considered the most repeated abnormal condition occurring in GCPV systems. Because these effects are caused by LG faults which is the most frequent type of fault in the power system. Thus, the control strategy of GCPV systems should be designed to perform stable operation under these disturbances.

In [33] the robustness of the control system was improved by applying sliding-mode control linked with the feedback linearization. The developed control method was implemented for single stage system to improve the dynamic performance. For realisation of the presented system reactive power was injected during LVRT operation which requires additional control conditions. Moreover, the control strategy was implemented for single stage method though dynamic performance becomes more important in two stage GCPV systems because of multiple control loops and parallel operation of several controllers.

Accordingly, the key objective of this paper is to propose an advanced control system to enhance stability of GCPV systems under normal and abnormal conditions. The proposed scheme was validated on a large-scale GCPV system having installed capacity of 2 MW. Initial parameters were calculated based on the equations and were tuned to meet the generation capacity of the large scale of proposed system. Furthermore, the findings proved that the developed control system is successfully maintained the stability of the system during short circuit fault conditions. This is significant for renewable energy systems and more broadly for modern power systems. An in-depth FFT analysis was initially performed to monitor voltage quality at the CCP under normal operation. The results showed that, with the developed control system, Total Harmonic Distortion (THD) at the CCP is well below the standard level defined in the IEEE Std. 519 [34]. The main contributions of the work are summarized as:

- A Voltage Source Converter (VSC) control system is modified and validated for a large-scale PV system during steady state conditions.
- Ability and performance of the designated control system is validated during short circuit fault. To this end, a L-G fault condition was applied at the grid side and an in-depth analysis was carried out to evaluate the control scheme.
- A comprehensive analysis of the LVRT was undertaken to prove the capability of the modified VSC control strategy for voltage stability of the same system during fault conditions.

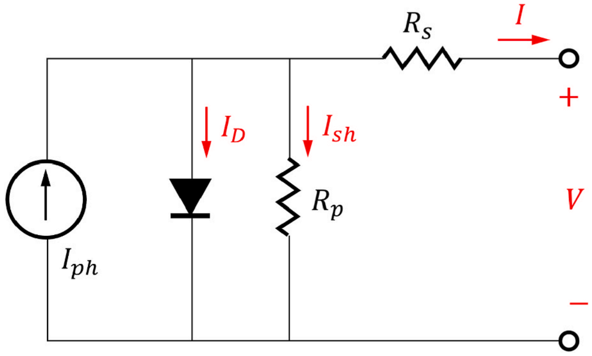

Fig. 2. Single diode structure of the PV cell.

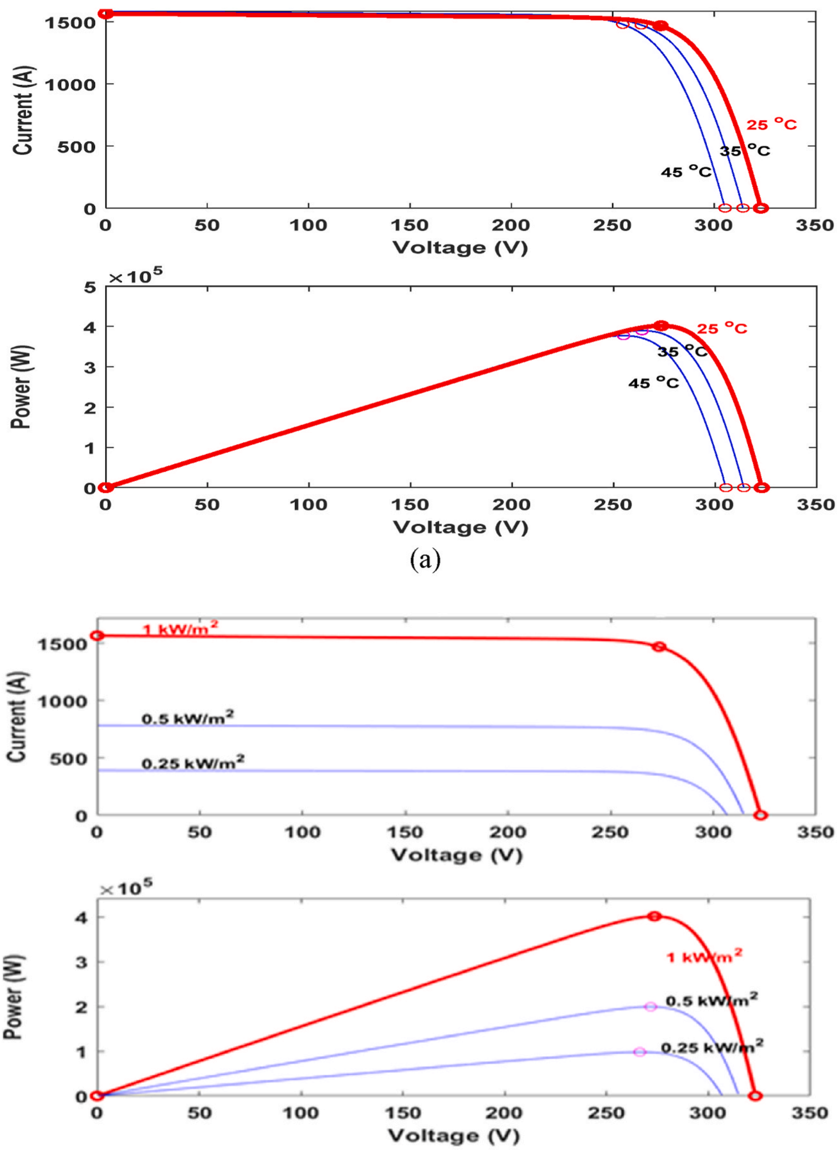

Fig. 3. The I–V and P–V characteristic of the PV array (a) at varying temperature (b) at varying irradiance.

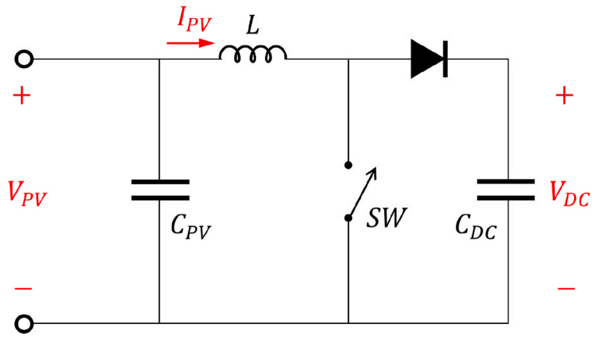

Fig. 4. The average model of boost converter.

In this study and associated analysis, L-G fault is considered predominantly in line with the UK regulations and LVRT grid code.

2. System description

A three phase two stages GCPV system was designed using the Simscape Electrical toolbox of MATLAB/SIMULINK; Fig. 1 exhibits a schematic diagram of the simulated system. This system composes of a PV array, DC-DC boost converter, control part for MPPT, inverter with VSC control, LC filter and step-up power transformer.

The PV generator consists of five parallel units, with rated power of 400 kW each and 2 MW in total. Each PV array comprises of 255 shunt strings and 5 modules coupled in every string. The PV module employed in the presented system is SunPower SPR-315E-WHT-D including a highest power rating of 315 W per module. Applied constraints of the PV module are displayed in Table 1.

A single solar cell is the fundamental element for solar PV generator scheme. An assembly of PV cells mounted on a framework forms a solar panel, also known as PV module. A combination of the PV modules connected in series and shunt arrangement constructs a complete PV array. Fig. 2 shows a basic circuit diagram of a solar cell circuit [17].

From the circuit diagram of Fig. 2, current supplied by each PV cell is given in equation (1):

$$I = I_{ph} - I_D - I_{sh} \tag{1}$$

where, I gives the current produced using a solar cell, I_{Ph} gives the photon current, I_D indicates the value of diode current and I_{SH} represents current magnitude passing in the parallel resistor R_P, while R_S is the series resistance of a PV cell [35]. Total current supplied by a PV array is defined by equation (2) [36,37]:

$$I = N_P I_{Ph} - N_P I_O \left[exp\left(\frac{\frac{V+I\,R_S}{N_S}}{a\,N\,V_{th}} \right) - 1 \right] - \left(\frac{V + I\,R_S}{R_P} \right) \tag{2}$$

where N_S and N_P are number of solar cells arranged in series and parallel configuration in each PV array, I_O gives the value of reverse saturation current, a indicates the diode ideality factor while V_{th} represents the thermal voltage. These constraints are controlled by the solar irradiance value, cell temperature, and reference values. The reference values for PV modules are usually given by the manufacturers at a standard test condition having irradiance level of 1000 W/m^2 and temperature value of 25 °C [38]. The I–V and P–V characteristics of the PV array implemented in this work for different levels of solar irradiance and temperature values are exhibited in Fig. 3 (a) and (b), respectively.

Second part of the system is the DC-DC boost converter which is implemented to boost the voltage magnitude supplied by the PV array. A DC-DC boost converter is responsible to boost the DC voltage level produced by the PV array, as well as to create a channel to apply the MPPT technique which improve the voltage quality and controllability of the system [39,40]. For the presented system, the average model of boost converter was used in which supply voltage was precisely controlled according to the reference voltage for developing the function of the converter. An equivalent circuit of the boost converter is illustrated in Fig. 4 [41]. The generated signal of the boost converter is controlled by the MPPT unit which regulates the duty cycle for the converter [42]. The following equation (3) is applied to obtain the duty cycle for boost converter:

$$D = 1 - \frac{V_{PV}}{V_{DC}} \tag{3}$$

Inductance and capacitance for the boost converter design are specified as given in equations (4) and (5) [5]:

$$L = \frac{V_{DC} \times D(1 - D)}{\Delta I_{DC} \times f} \tag{4}$$

Table 1
Parameters of the PV module.

SunPower SPR-315E -WHT-D		
Parameter	Value	Unite
Maximum Power	315	W
Cells per module	96	–
Open Circuit Voltage	65	V
Short circuit current	6	A
Voltage at maximum power point	55	V
Current at maximum power point	6	A
Temperature coefficient of V_{oc}	−0.2727	°C
Temperature coefficient of I_{sc}	0.0617	°C
Diode ideality factor	0.9507	–
Series Resistance	0.4304	Ω
Shunt Resistance	430	Ω

Table 2
Parameters of the boost converter.

Parameter	Symbol	Value
Input Voltage	V_{PV}	273 V
Output Voltage	V_{DC}	500 V
Inductor	L	5 mH
Input Capacitor	C_{PV}	100 μF
Output Capacitor	C_{DC}	2 F

Output of the DC-DC converter is delivered to the inverter which transforms the DC voltage to a Pulse Width Modulation (PWM) voltage signal. The obtained signal at the output of the inverter is then filtered via harmonic filter for suppression of higher frequency components and to get THD of the current and voltage below 5 % standard level as stated by the IEEE std.519 [34–43].

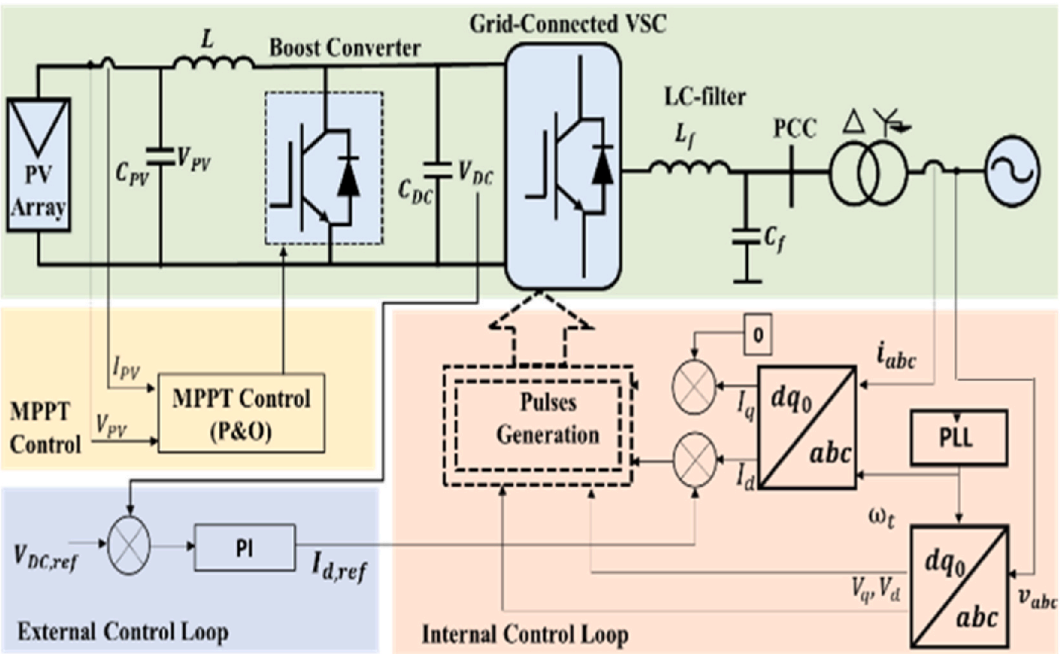

Fig. 5. Block diagram of the control system of the GCPVS.

$$C_{DC} = \frac{V_{PV} \times D(1-D)}{8Lf^2 \Delta V_c} \tag{5}$$

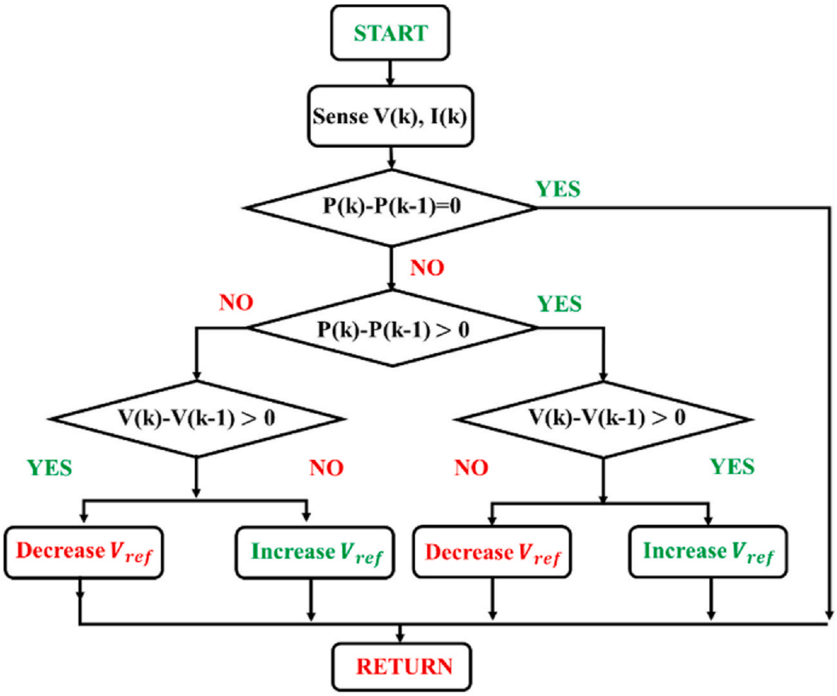

Fig. 6. Flowchart for P&O MPPT technique.

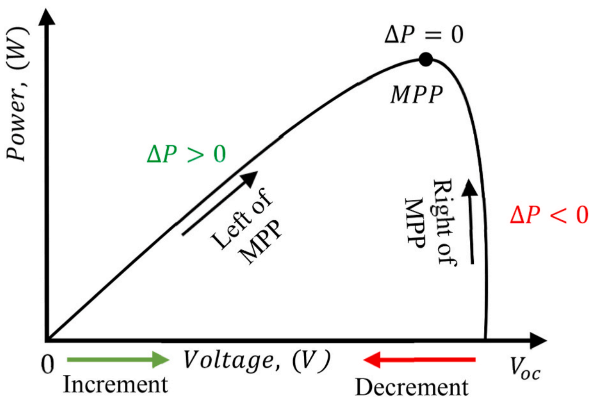

Fig. 7. PV characteristics of P&O MPPT technique.

where V_{DC} is voltage at the terminal of the DC-DC boost converter and I_{DC} indicates the value of the current supplied to the inverter. V_{DC} is determined with reference to the input voltage V_{PV} and the duty cycle of the converter. The parameters used for this boost converter are demonstrated in Table 2 which are calculated applying equations (4) and (5).

3. Control system strategy

A schematic diagram of the established control scheme is explained in Fig. 5. This control unite comprises of two main parts: DC controller based on MPPT algorithm, and VSC control scheme for the inverter. These two parts are described in the succeeding subsections.

3.1. MPPT control scheme

The control system on the DC side is designed for maximum power extraction and to increase the voltage level of the PV array. A Perturb and Observe (P&O) algorithm based MPPT scheme was used for MPPT operation. Considering the output voltage and current signals of the PV array, the P&O algorithm determines the duty cycle of the DC-DC converter. A flowchart of the P&O algorithm is

Table 3
Principle of the P&O algorithm.

Perturbation	Change in Power	Next perturbation
Positive	Positive	Positive
Positive	Negative	Negative
Negative	Positive	Negative
Negative	Negative	Positive

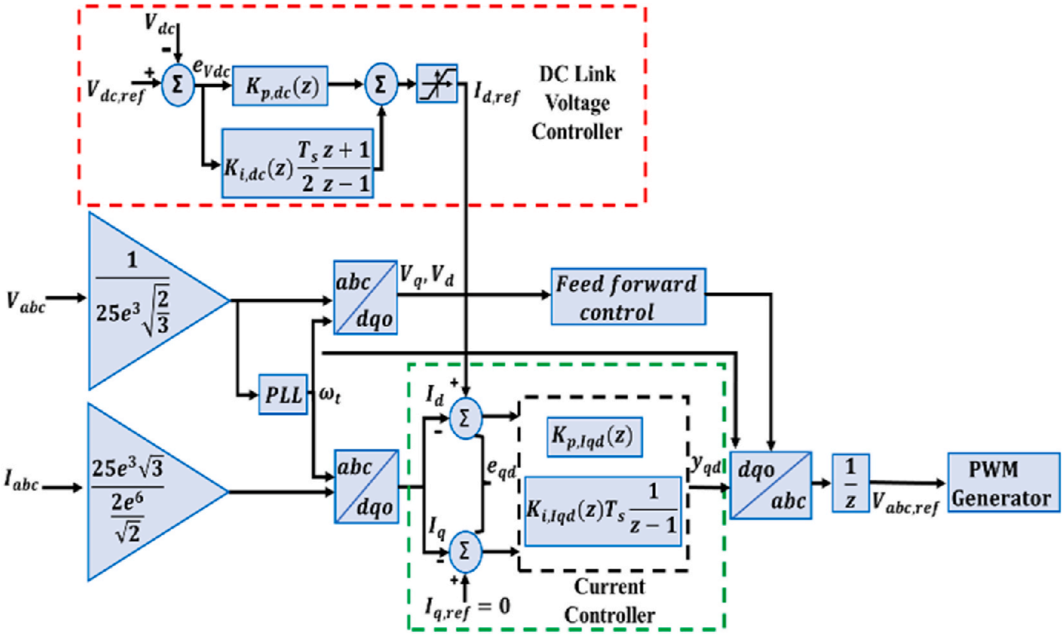

Fig. 8. Block diagram of VSC control strategy.

shown in Fig. 6.

This algorithm determines the duty cycle of the DC-DC boost converter based on the input parameters, i.e., voltage and current from the PV array. Output voltage of the boost converter is regulated according to the reference values. The MPPT technique and associated algorithm are implemented to get the maximum power delivered by the PV array and output power of the system is maintained with reference to the voltage variation [15]. In this control scheme, voltage is perturbed according to the response of the system to the previous perturb to decide the direction of the following perturbation [44]. PV characteristic curve and principle of the P&O based MPPT technique are demonstrated in Fig. 7 and Table 3, respectively.

For $\Delta P > 0$, power is increased with increasing the voltage until MPP is achieved. After attaining MPP, where $\Delta P < 0$, any attempt to increase the voltage results in decreasing the power. Accordingly, if increasing or decreasing the voltage led to an increase in the power output, the successive perturbation continues the same direction until MPP is achieved. On the other hand, if power decreases with the increase or decrease in voltage, the following perturbation will be reversed, as shown in Table 3. After reaching the MPP, the system will be continuously oscillating around this point. Level of the fluctuations across the MPP alters with reference to the step size of the supplied voltage. However, to decrease these fluctuations, reduced step-size can be applied, which may slow down the MPPT process to reach the MPP [44].

3.2. *Control scheme of the Voltage Source Converter*

A block diagram of the designed control system of the VSC is presented in Fig. 8. In this control system, the VSC-based control scheme is synchronized to the CCP using phase locked loop (PLL) unit which generate a reference angle ω_t [45]. The error signal e_{Vdc} between the DC link voltage, generated by comparing V_{dc} and its corresponding reference value $V_{dc,ref}$, is fed to the compensator whose output u_{Vdc} is processed by a limiter to generate reference current value $I_{d,ref}$.

For this system the transfer function of the control unit was determined using Z transformation, so the output U_{Vdc} can be presented mathematically as defined in equations (6)–(8) [28]:

$$U_{Vdc}(z) = E_{Vdc}(z)\left[K_{p,dc}(z) + K_{i,dc}(z)\left(\frac{T_s}{2}\frac{z+1}{z-1}\right)\right] \tag{6}$$

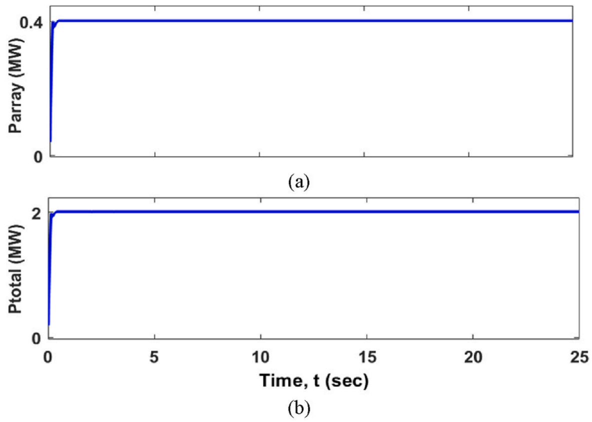

Fig. 9. Output power of the PV system (a) single array (b) five arrays in parallel.

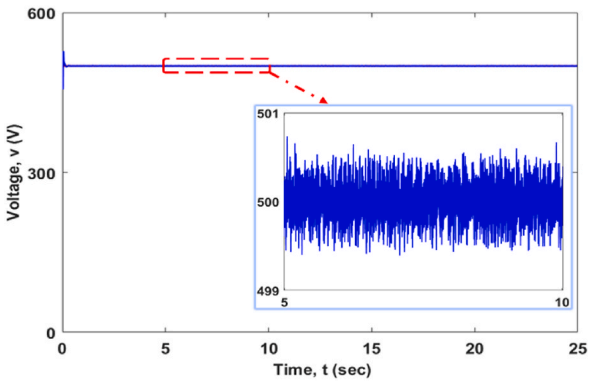

Fig. 10. DC Voltage at the DC link bus bar.

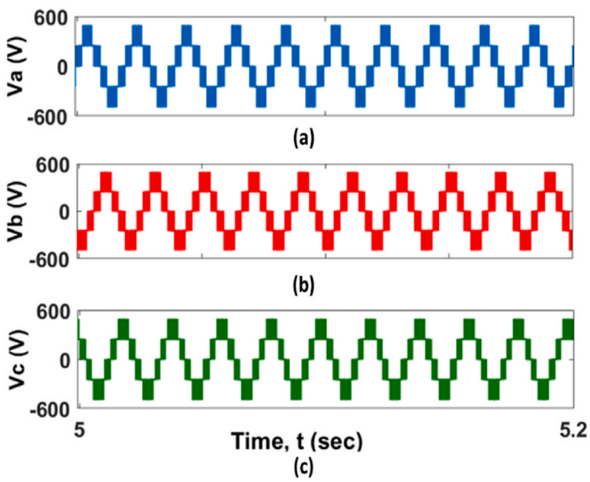

Fig. 11. Phase voltage at the terminal of the PWM inverter (a) phase A (b) phase B (c) phase C.

where:

$$e_{Vdc} = V_{DC} - V_{DCref}, U_{Vdc}(z) = Z(u_{Vdc}) \tag{7}$$

and

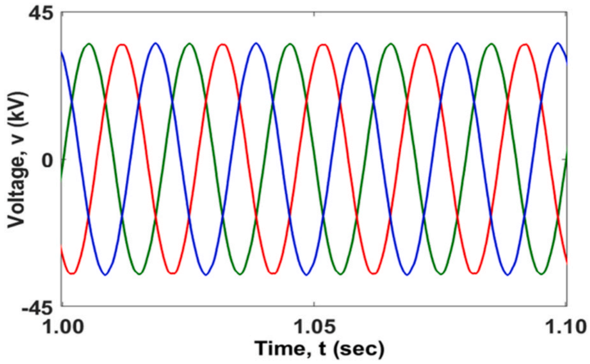

(a)

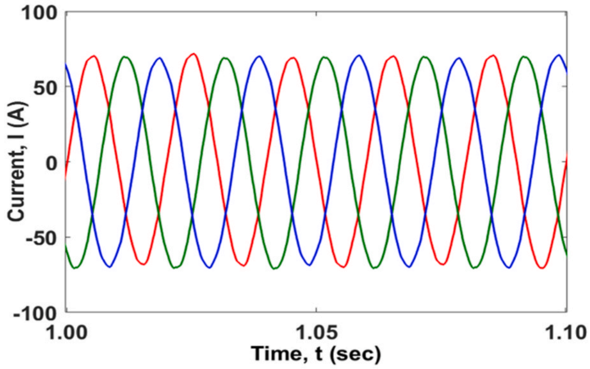

(b)

Fig. 12. Instantaneous wave shapes of three phase (a) voltages and (b) currents at CCP.

$$E_{Vdc}(Z) = Z(e_{Vdc}) \tag{8}$$

The reference signal $I_{d,ref}$ is then delivered to the current controller block. Three phase grid voltage V_{abc} and current I_{abc} are attained from the grid and converted to per unit values. After conversion, these signals are converted to $dq0$ reference, which is presented as (V_d, V_q) and (I_d,I_q) for the voltage and current, respectively. Voltage components V_d and V_q are then processed for feed forward control, which play a crucial function in improving the stability of the PV system by offsetting the nonlinear characteristics of the PV arrays. The *d-q* parts of the current, I_d and I_q, are then processed through the PI controller. For this purpose, the signals are compared with reference values, $I_{d,ref}$ and $I_{q,ref}$. These I_d and I_q components are decoupled for decoupled control of the active and reactive power respectively. The presented system was operated at unity power factor, so $I_{q,ref}$ is set to zero [46,47]. Reference current $I_{d,ref}$ is gained from the external control loop based on the values of V_{dc} and $V_{dc,ref}$ and is compared with the *d*-component of the grid currents, I_d. Current reference value obtained from DC control block $I_{d,ref}$ was used to track the signal I_d and to produce error signal e_{qd}. The gained error signal is processed by the respective controller to provide the output signal y_{qd} of the current controller which can be given in equations (9) and (10):

$$Y_{qd}(z) = E_{qd}(z)\left[K_{p,Iqd}(z) + K_{i,Iqd}(z)\left(T_s\frac{1}{z-1}\right)\right] \tag{9}$$

where:

$$Y_{qd}(z) = Z\left(y_{qd}\right) \text{ and } E_{qd}(z) = Z\left(e_{qd}\right) \tag{10}$$

The output y_{qd} represents the signal to generate reference voltage $V_{abc,ref}$ which is delivered to the PWM generator to generate pulses signals for the inverter operation.

4. Results and discussion

Dynamic performance of the GCPV solar system was evaluated under two different conditions: steady state operation, and L-G short circuit fault condition. Results of each study is presented and discussed in the following subsections.

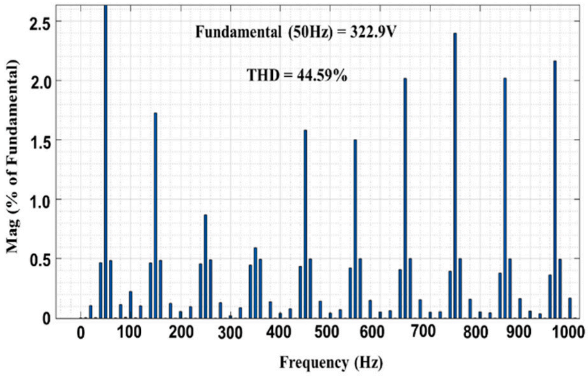

(a)

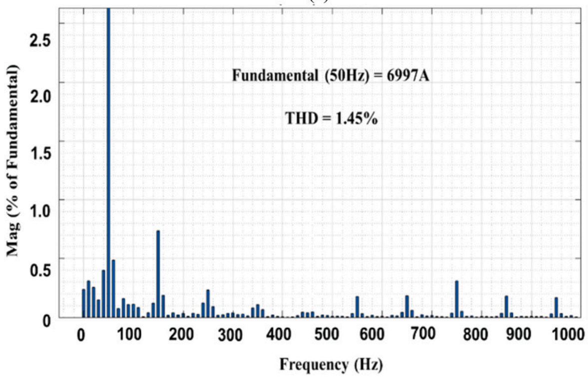

(b)

Fig. 13. Frequency spectrum and THD level of (a) voltage and (b) current at the inverter terminal.

4.1. Steady state operation

In this stage the system was operated at Standard Test Conditions (STC) with solar irradiance level of 1000 W/m^2 and ambient temperature value of 25°C. The power generated by a single PV array and five PV arrays assembled in parallel, are shown in Fig. 9-a and 9-b, respectively. The results show that the system operates at its full capacity and delivers maximum power, which verify that the controller of the DC-DC boost converter works effectively to track the MPP of the PV system. It is important to highlight that the P&O algorithm has been implemented for MPPT control to confirm that maximum power is delivered from the system by maintaining the optimized points of the PV characteristics curve of the PV arrays.

In the second stage of this study, voltage at the DC busbar was monitored, the result is presented in Fig. 10. The DC-DC boost converter with the designated control strategy of the MPPT algorithm, successfully boost the DC voltage produced by the PV arrays from 273.5 V to 500 V. Fig. 10 clearly shows that voltage at the DC busbar follows the reference voltage that has been set by the DC voltage regulator of the inverter. Furthermore, the oscillation of the DC voltage across the reference value is less than $\pm$ 0.5 V, this means the DC voltage supplied to the PWM inverter is effectively regulated. This will ensure a stable AC voltage at the inverter terminal as well as the enhanced stability of the whole system.

A 3-level PWM inverter with a nominal frequency of 50 Hz, synchronized with the grid power frequency was employed. The designated control scheme monitors and controls the switching function of the inverter using phase angle and frequency of the grid voltage as reference values. Three phase voltages at the inverter terminal are illustrated in Fig. 11(a – c).

In the last stage of the GCPV system and before integrating at the grid side, a LC filter was implemented to filter the high-frequency harmonics generated by the PWM inverter. To this end, parameters of the LC filter were determined to bring the THD level well below 5 %, which comply with the IEEE Std. 519 [43]. Three phase voltage and current signals at the CCP are represented in Fig. 12-a and 12-b, respectively. A FFT analysis was performed to examine the THD values for the voltage and the current signals at different points across the system.

Frequency spectrum and THD level for the current and voltage at the inverter terminal and CCP are presented in Fig. 13 and 14, respectively. It can be noted from Fig. 13 (a) and (b) that the THD values of the voltage and current at the inverter terminal, before the LC filter, are 44.59 % and 1.45% respectively. While the THD values of the voltage and current signals at the CCP were recorded 1.68 % and 1.37 %, respectively as shown in Fig. 14 (a) and (b); which is well below the acceptable level as stated in the IEEE Std. 519 [43].

This explicitly highlights the effective operation of the LC filter to reduce the THD values of the voltage at the CCP. Finally, the PV system was integrated with the gride using a step-up power transformer.

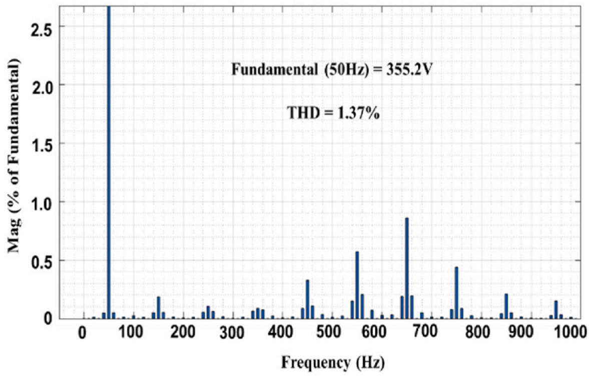

(a)

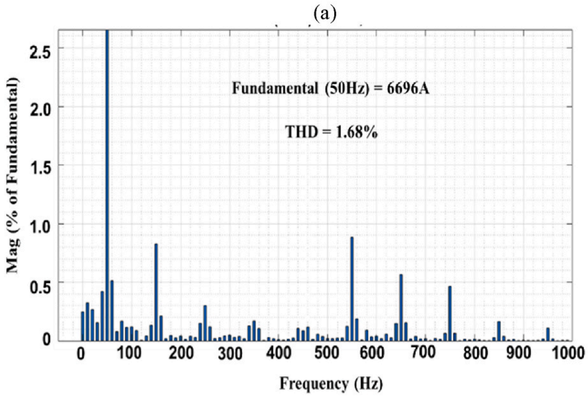

(b)

Fig. 14. Frequency spectrum and THD values of (a) voltage and (b) current at CCP.

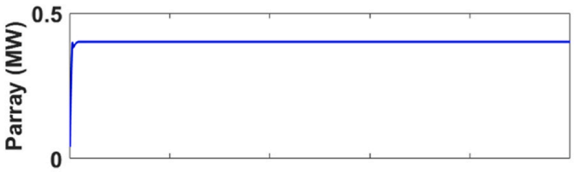

(a)

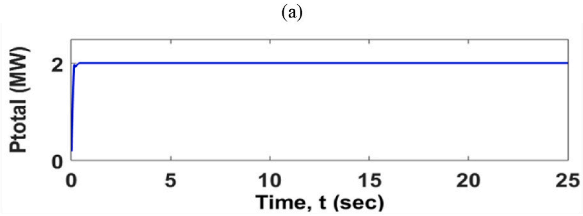

(b)

Fig. 15. Output power of the PV system with a L-G fault in place (a) single array (b) five arrays in parallel.

4.2. Short circuit faults analysis

As the key objective of this work, dynamic behaviour of the system under transient fault condition was studied. For this purpose, a L-G short circuit fault, as the most frequent fault in practical power systems, was considered. This fault was introduced to the secondary side of the step-up transformer at $t = 2$ *sec* for a duration of 1 *sec*. The produced power by the PV arrays during the transient fault condition was initially monitored, the results are shown in Fig. 15 (a) and (b).

Fig. 15 exhibits that the delivered power at the output side of the PV array is not affected by this short circuit fault. This explicitly verifies the efficiency of the designed control approach to maintain the nominal power delivered by the system as the same operating point during normal operation. This implies that, with the designated control strategy in place, this kind of fault has negligible impact

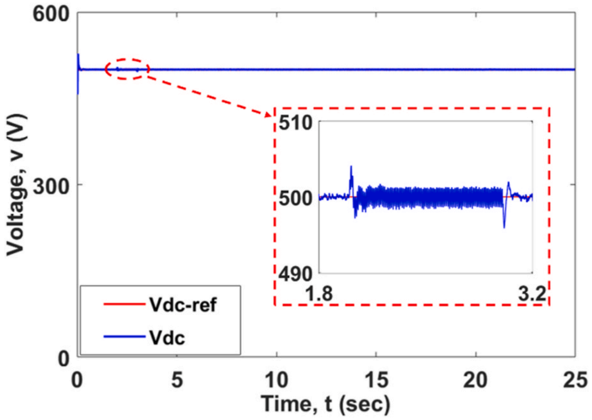

Fig. 16. DC link Voltage under L-G fault.

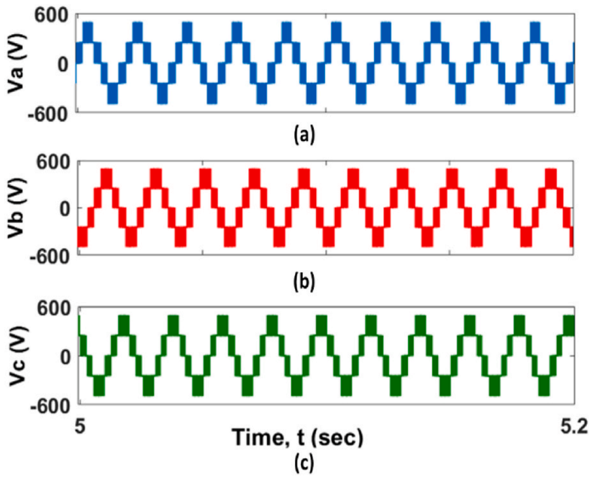

Fig. 17. Three phase voltage at inverter terminal with a L-G fault in place (a) phase A (b) phase B (c) phase C.

on the voltage and current output generated by the PV arrays, and therefore on the DC side of the system. This evidently shows that the designated control system successfully protects the PV system from the undesirable impacts of short circuit faults. This is an essential criterion for maintaining the normal function of the PV system during L-G fault conditions.

Voltage at the DC busbar was then monitored, the result is exhibited in Fig. 16. As can be seen the concerned fault at the grid side makes a minor impact on the DC link voltage. From this outcome, the magnitude of the oscillations increased instantly at $t = 2$ *sec*, when the fault is applied, but overshoot of the voltage is limited to about ± 5 *V*. However, the system regained its stability within a very short time of as low as 0.2 *sec*, after the fault is cleared. At $t = 3$ *sec*, when the fault is cleared, the DC voltage fluctuations increased for a short period, and restored to its normal operation within 0.15 *sec*.

These findings show the capability of the designed control system for maintaining the voltage stability at the DC busbar. However, when it comes to the AC side of the system, the L-G fault impacts on the voltage and current are higher than that on the DC side. The instantaneous waveforms of the three-phase voltage at the inverter terminal are shown in Fig. 17 (a – c). Impact of the concerned fault on the instantaneous waveforms and rms ratings of three-phase current and voltage signals at the CCP are illustrated in Figs. 18–21, respectively. Fig. 18 (a) illustrates the impact of the applied fault on current signal at CCP which was started at point A and cleared at point B while Fig. 18 (b) and (c) present the zoomed views of respective points.

Three phase rms currents I_a, I_b and I_c at CCP under L-G fault are presented in Fig. 19(a–c) respectively. Accordingly, the instantaneous three phase voltage signals are shown in Fig. 20 (a) while Fig. 20 (b) and (c) show the zoomed views of the points when the fault was applied and cleared respectively. Whereas Fig. 21(a–c) present the three phase rms voltages V_a, V_b and V_c under L-G fault respectively.

In the presented VSC based control strategy, a control system is designed in accordance with the feedback from the grid side parameters as shown in Fig. 8, due to the required synchronization of both systems. So, as a fault arises at the grid side, it has immediate impact on the GCPV system parameters and disrupts its normal operation.

The results show that, impact of the applied fault on voltage and current at the CCP is more severe, which comply with the theory of

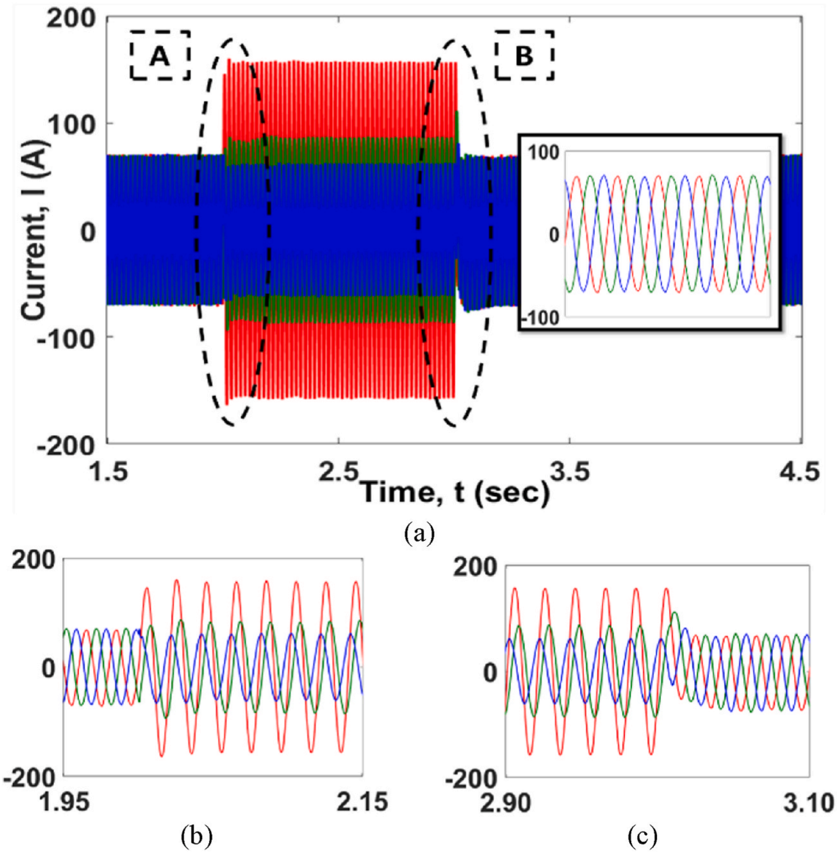

Fig. 18. Instantaneous waveforms of three phase currents at CCP under L-G fault (a) complete waveforms (b) transient currents after applying the fault at point A and (c) transient currents when the fault is cleared at point B.

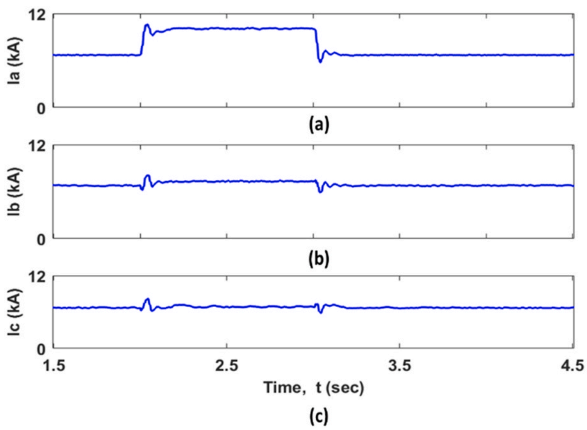

Fig. 19. Three phase rms currents at CCP under L-G fault (a) phase A (b) phase B (c) phase C.

transient fault conditions in the conventional power systems [48]. However, with the designated control system in place, currents and voltage in all three phases returned to the normal value in a settling time of as low as 0.15 *sec*.

Based on the grid codes requirements, the GCPV system waits for a particular period whether fault to be cleared; if so, system parameters regain the normal operation based on the feedback signals from the gird. In contrast, if the faults are prolonged, system is disconnected to prevent severe damages. The voltage and current signals at the grid side clearly show that the fault condition is immediately reflected in the parameters of the GCPV system and caused the voltage sag and increased current at the same instant when the fault occurred. On the other hand, the negligible impact of the applied fault on the DC part of the system can be attributed to the

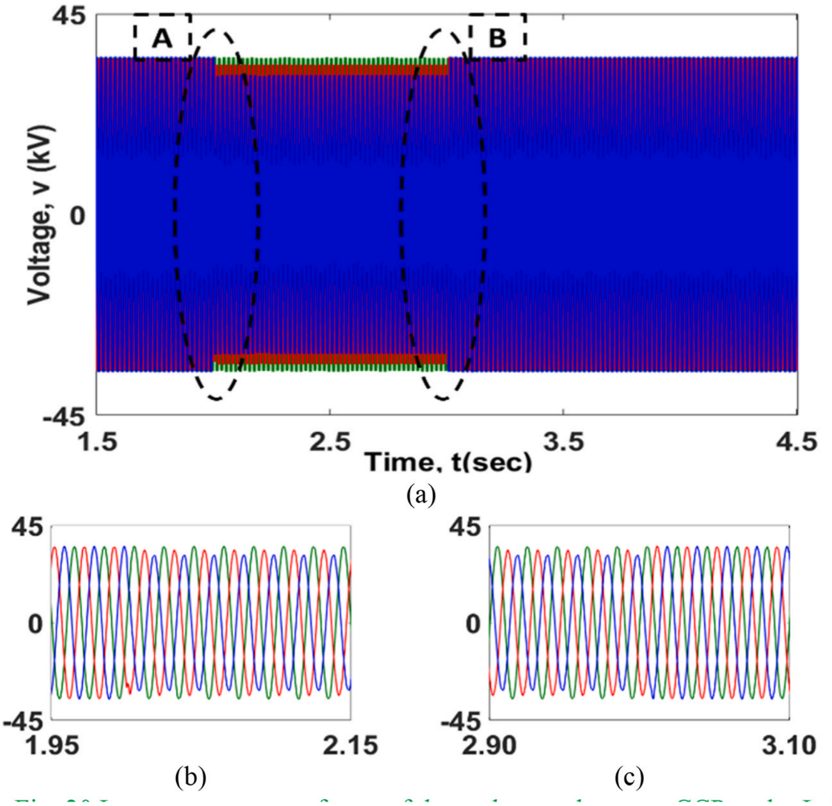

Fig. 20. Instantaneous waveforms of three phase voltages at CCP under L-G fault (a) complete waveforms (b) transient voltages after applying the fault at point A and (c) transient voltages when the fault is cleared at point B.

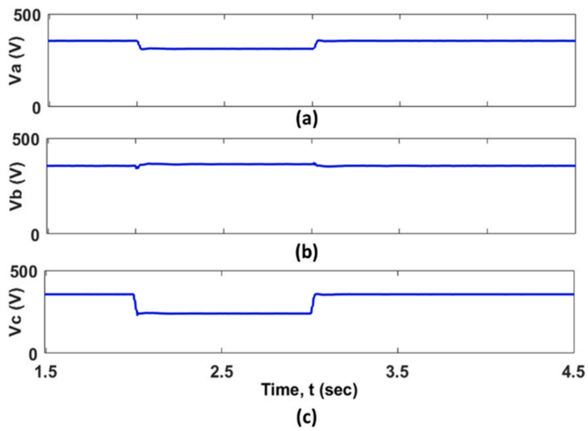

Fig. 21. Three phase rms voltages at CCP under L-G fault (a) phase A (b) phase B (c) phase C.

position of the fault and the role played by different impedance levels for various components of the system, including transmission lines, transformers, and harmonic filters. These components help in mitigating the impacts of the applied faults. From this analysis it is evident that getting feedback from the grid side supports the overall function of the GCPV system as it is important to monitor the grid conditions while the PV system is in operation and has great impact on the grid parameters.

4.3. LVRT capability analysis

Short circuit faults impose voltage dip, and the grid requirements to maintain connected during the fault period is defined by means of LVRT [9,10]. In this work, the LVRT capability of the modelled GCPV system has been analysed in line with the UK grid code.

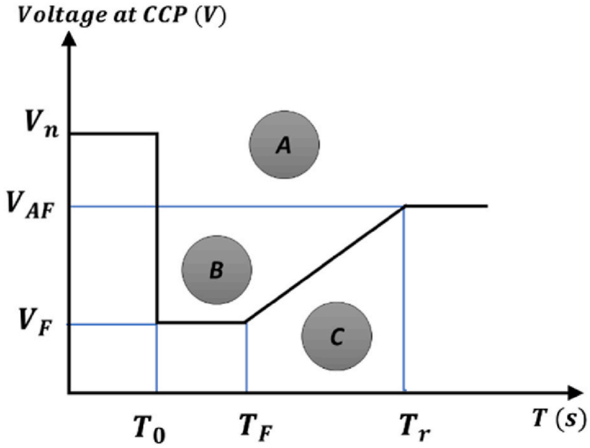

Fig. 22. General curve limits of LVRT.

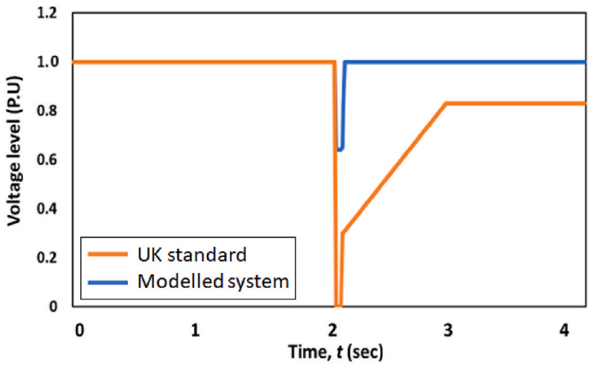

Fig. 23. Comparison of LVRT of the modelled system and UK requirement.

Considering the rapid development of grid connected RESs, LVRT becomes a mandatory requirement and have been broadly adopted in the grid codes of modern power systems. This concept is shown graphically in Fig. 22. In this graph, V_n indicates nominal voltage, V_F shows voltage during the period of fault, V_{AF} represents voltage after fault, and T_F and T_r denote the period at which voltage dipped because of fault and recovery time, respectively. According to the LVRT requirement, the GCPV system tolerates voltage sags to a specific ratio of the rated voltage for a certain period, as shown in Fig. 22 [49].

In Fig. 22, area Ⓐ indicates the normal operation of the GCPV system at the CCP. If the voltage magnitude at CCP falls in area Ⓑ, GCPV remains connected for a certain time (T_0 to T_F), and it should also have ability to regain nominal voltage magnitude at a certain rate. In area Ⓒ, GCPV system is allowed to be disconnected. Rate of change of the voltage varies depending upon the grid regulations for different countries. L-G faults, as the most frequent type of fault in the power system, cause severe voltage sags. Therefore, it is crucial to analyse the LVRT capability of GCPV systems for the optimized setting and coordination of protection equipment.

To analyse the LVRT capability of the modelled system, a L-G fault was applied at the CCP for a duration of 140 ms, which is recommended duration for this test [11]. Voltage profile was then monitored and analysed to assess the LVRT capability of the simulated system, the results in comparison with the UK standard is shown in Fig. 23.

It can be observed that at the instant when fault occurred, voltage at CCP drops to 0.7 p.u. causing the voltage sag throughout the fault duration till 140 ms. It is important to highlight that according to the UK standard [11], nominal voltage can drop to zero during fault condition but for the modelled system, voltage value was maintained at a higher magnitude reducing the severity of voltage sag at CCP. After 140 ms of fault duration, voltage restored to its pre fault value, which is at a higher rate within 20 ms, for the modelled system, as compared to the minimum standard rate of the UK requirement. This validates the ability of the control system for stable and quicker operation of the system".

5. Conclusions

In this paper a dynamic model was developed for a grid connected solar PV system having power production capacity of 2 MW. Dynamic function of the designed system was studied under steady state and transient fault conditions. Two control systems, one for controlling the function of DC-DC boost converter, and the other one to control the VSC were designed and implemented. The key function of the DC-DC controller is to achieve MPP, while the VSC controller is to maintain voltage quality at the CCP, and stability of the system during short circuit faults. The results showed that, the designated control systems can effectively provide clean voltage at the CCP with a THD of 1.39 %, which is well below the threshold level of the IEEE Std. 519.

As a key objective of this work, dynamic performance of the system subjected to a L-G fault at the CCP was evaluated, as well as LVRT analysis was also considered. The results showed that, with the designated control schemes in place, performance of the PV side including voltage at the DC busbar and MPPT were not affected by the concerned short circuit fault. More importantly, the system is capable to regains its stability when the fault is disappeared having a settling time of less than 0.2 sec.

Data availability statement

Data included in article/supp. material/referenced in article.

Additional information

No additional information is available for this paper.

CRediT authorship contribution statement

Hussin Zahloul: Writing – review & editing, Writing – original draft, Validation, Software, Methodology, Investigation, Formal analysis. **Arjmand Khaliq:** Writing – review & editing, Writing – original draft, Validation, Software, Methodology, Investigation, Formal analysis. **Hamed Hamzehbahmani:** Writing – review & editing, Supervision, Methodology. **Sergii Veremieiev:** Writing – review & editing, Supervision. **Sana Salous:** Writing – review & editing, Supervision.

Declaration of competing interest

The authors declare that they have no known competing financial interests or personal relationships that could have appeared to influence the work reported in this paper.

Acknowledgements

This paper is based on PhD research projects which are funded by Libyan government for author[1] and by Commonwealth Scholarship commission and the foreign, Commonwealth and development office in the UK for author[2]. We are grateful for their support. All views here are those of the authors[1,2]not the funding bodies.

References

[1] M.A. Eltawil, Z. Zhao, Grid-connected photovoltaic power systems: technical and potential problems-A review, Renew. Sustain. Energy Rev. 14 (1) (2010) 112–129, https://doi.org/10.1016/j.rser.2009.07.015.
[2] L. A, et al., Smart energy monitoring and power quality performance based evaluation of 100-kW grid tied PV system, Heliyon 9 (6) (2023) e17274, https://doi.org/10.1016/j.heliyon.2023.e17274.
[3] G. Rajgor, Greater acceleration of renewables required to meet COP21 goal, Renew. Energy Focus 17 (5) (2016) 175–177, https://doi.org/10.1016/j.ref.2016.08.007.
[4] T. Ruan, M. Topel, W. Wang, B. Laumert, Potential of grid-connected decentralized rooftop PV systems in Sweden, Heliyon 9 (6) (2023) e16871, https://doi.org/10.1016/j.heliyon.2023.e16871.
[5] S. Sumathi, L. Ashok Kumar, P. Surekha, Solar PV and Wind Energy Conversion Systems, 2015.
[6] N.A. Mehedi Fahad, Mohammed Ali, Nahar Islam, A New Approach to Design of an Optimized Grid Tied Smart Solar, vol. 1, 2012, pp. 3–7.
[7] D.B. Aeggegn, T.F. Agajie, Y.G. Workie, B. Khan, A. Fopah-Lele, Feasibility and techno-economic analysis of PV-battery priority grid tie system with diesel resilience: a case study, Heliyon 9 (9) (2023) e19387, https://doi.org/10.1016/j.heliyon.2023.e19387.
[8] A.K. Shukla, K. Sudhakar, P. Baredar, Simulation and performance analysis of 110 kWp grid-connected photovoltaic system for residential building in India: a comparative analysis of various PV technology, Energy Rep. 2 (2016) 82–88, https://doi.org/10.1016/j.egyr.2016.04.001.
[9] R.T. Juarez, C.R. Fuerte-Esquivel, E. Espinosa-Juarez, U. Sandoval, Steady-state model of grid-connected photovoltaic generation for power flow analysis, IEEE Trans. Power Syst. 33 (5) (2018) 5727–5737, https://doi.org/10.1109/TPWRS.2018.2817585.
[10] A. Chidurala, T.K. Saha, N. Mithulananthan, Harmonic impact of high penetration photovoltaic system on unbalanced distribution networks - learning from an urban photovoltaic network, IET Renew. Power Gener. 10 (4) (2016) 485–494, https://doi.org/10.1049/iet-rpg.2015.0188.
[11] M. Yadav, N. Pal, D.K. Saini, Low voltage ride through capability for resilient electrical distribution system integrated with renewable energy resources, Energy Rep. 9 (2023) 833–858, https://doi.org/10.1016/j.egyr.2022.12.023.
[12] I. Yahyaoui, Advances in Renewable Energies and Power Technologies: Solar and Wind Energies, Elsevier, 2018.
[13] J. Mohammadi, S. Afsharnia, S. Vaez-Zadeh, Efficient fault-ride-through control strategy of DFIG-based wind turbines during the grid faults, Energy Convers. Manag. 78 (2014) 88–95, https://doi.org/10.1016/j.enconman.2013.10.029.
[14] T. Qoria, X. Wang, R. Kadri, Grid-forming control VSC-based including current limitation and re-synchronization functions to deal with symmetrical and asymmetrical faults, Electr. Power Syst. Res. 223 (2022) (2023) 109647, https://doi.org/10.1016/j.epsr.2023.109647.
[15] A.I.M. Ali, M.A. Sayed, E.E.M. Mohamed, Modified efficient perturb and observe maximum power point tracking technique for grid-tied PV system, Int. J. Electr. Power Energy Syst. 99 (2018) 192–202, https://doi.org/10.1016/j.ijepes.2017.12.029.
[16] L.P. Sampaio, M.V. Da Rocha, S.A.O. Da Silva, M.H.T. De Freitas, Comparative analysis of MPPT algorithms bio-inspired by grey wolves employing a feedforward control loop in a three-phase gridconnected photovoltaic system, IET Renew. Power Gener. 13 (8) (2019) 1379–1390, https://doi.org/10.1049/iet-rpg.2018.5941.
[17] A.K. Verma, B. Singh, Harmonics and reactive current detection of a grid-interfaced PV generation in a distribution system, IEEE Trans. Ind. Appl. 54 (5) (2018) 4786–4794, https://doi.org/10.1109/TIA.2018.2830752.

[18] L.B.G. Campanhol, S.A.O. Da Silva, A.A. De Oliveira, V.D. Bacon, Power flow and stability analyses of a multifunctional distributed generation system integrating a photovoltaic system with unified power quality conditioner, IEEE Trans. Power Electron. 34 (7) (2019) 6241–6256, https://doi.org/10.1109/TPEL.2018.2873503.
[19] A. Khaliq, H. Zahloul, H. Hamzehbahmani, A control approach for power quality improvement of a large-scale grid connected PV system at standard test conditions 1 (2022) 241–245, https://doi.org/10.1049/icp.2022.1836.
[20] S. Silvestre, M.A. Da Silva, A. Chouder, D. Guasch, E. Karatepe, New procedure for fault detection in grid connected PV systems based on the evaluation of current and voltage indicators, Energy Convers. Manag. 86 (2014) 241–249, https://doi.org/10.1016/j.enconman.2014.05.008.
[21] T. Lin, M. Das, A. Gole, A. Isaacs, Adaptive fault ride through control of VSM Grid-forming converters, Electr. Power Syst. Res. 223 (December 2022) (2023) 109606, https://doi.org/10.1016/j.epsr.2023.109606.
[22] O. Goksu, R. Teodorescu, B. Bak-Jensen, F. Iov, P.C. Kjar, An Iterative Approach for Symmetrical and Asymmetrical Short-Circuit Calculations with Converter-Based Connected Renewable Energy Sources. Application to Wind Power, IEEE Power Energy Soc. Gen. Meet., 2012, pp. 1–8, https://doi.org/10.1109/PESGM.2012.6344906.
[23] R.K. Varma, S.A. Rahman, V. Atodaria, S. Mohan, T. Vanderheide, Technique for fast detection of short circuit current in PV distributed generator, IEEE Power Energy Technol. Syst. J. 3 (4) (2016) 155–165, https://doi.org/10.1109/jpets.2016.2592465.
[24] J.C. Das, Power System, Marcel Dekker, Inc., New York, 2002.
[25] B. Vahidi, S.A. Agheli, S. Jazebi, Teaching short-circuit withstand test on power transformers to M.Sc. students and junior engineers using MATLAB-SIMULINK, Comput. Appl. Eng. Educ. 20 (3) (2012) 484–492, https://doi.org/10.1002/cae.20416.
[26] H. Zahloul, H. Hamzehbahmani, A. Khaliq, S. Veremieiev, An approach to dynamic behaviour of a grid connected PV system during symmetrical short circuit fault, 2022 13th Int. Renew. Energy Congr. IREC (2022) 2022, https://doi.org/10.1109/IREC56325.2022.10002093.
[27] D.S. Pillai, J.P. Ram, N. Rajasekar, A. Mahmud, Y. Yang, F. Blaabjerg, Extended analysis on Line-Line and Line-Ground faults in PV arrays and a compatibility study on latest NEC protection standards, Energy Convers. Manag. 196 (April) (2019) 988–1001, https://doi.org/10.1016/j.enconman.2019.06.042.
[28] M. Graungaard Taul, X. Wang, P. Davari, F. Blaabjerg, Current reference generation based on next-generation grid code requirements of grid-tied converters during asymmetrical faults, IEEE J. Emerg. Sel. Top. Power Electron. 8 (4) (2020) 3784–3797, https://doi.org/10.1109/JESTPE.2019.2931726.
[29] M. Mirhosseini, J. Pou, V.G. Agelidis, Single- and two-stage inverter-based grid-connected photovoltaic power plants with ride-through capability under grid faults, IEEE Trans. Sustain. Energy 6 (3) (2015) 1150–1159, https://doi.org/10.1109/TSTE.2014.2347044.
[30] J. Joshi, A.K. Swami, V. Jately, B. Azzopardi, A comprehensive review of control strategies to overcome challenges during LVRT in PV systems, IEEE Access 9 (2021) 121804–121834, https://doi.org/10.1109/ACCESS.2021.3109050.
[31] M. Nasiri, A. Arzani, J.M. Guerrero, LVRT operation enhancement of single-stage photovoltaic power plants: an analytical approach, IEEE Trans. Smart Grid 12 (6) (2021) 5020–5029, https://doi.org/10.1109/TSG.2021.3108391.
[32] S. Landl, H. Kirchsteiger, Mitigating overvoltage in power grids with photovoltaic systems by energy storage, Environ. Clim. Technol. 26 (1) (2022) 470–483, https://doi.org/10.2478/rtuect-2022-0036.
[33] M. Almaktar, A.M. Elbreki, M. Shaaban, Revitalizing operational reliability of the electrical energy system in Libya: feasibility analysis of solar generation in local communities, J. Clean. Prod. 279 (2021) 123647, https://doi.org/10.1016/j.jclepro.2020.123647.
[34] IEEE Std 519, IEEE Recommended Practice and Requirements for Harmonic Control in Electric Power Systems Sponsored by the Transmission and Distribution Committee IEEE Power and Energy Society, vol. 2014, IEEE Stand., 2014, pp. 1–29.
[35] A.M. Humada, A.M. Aaref, H.M. Hamada, M. Herwan, Modeling and characterization of a grid-connected photovoltaic system under tropical climate conditions, Renew. Sustain. Energy Rev. 82 (2015) (2018) 2094–2105, https://doi.org/10.1016/j.rser.2017.08.053.
[36] A.M. Humada, A.M. Aaref, H.M. Hamada, M.H. Sulaiman, N. Amin, S. Mekhilef, Modeling and characterization of a grid-connected photovoltaic system under tropical climate conditions, Renew. Sustain. Energy Rev. 82 (2018) 2094–2105, https://doi.org/10.1016/j.rser.2017.08.053.
[37] H.A. Kazem, M.T. Chaichan, A.H.A. Al-Waeli, K. Sopian, A novel model and experimental validation of dust impact on grid-connected photovoltaic system performance in Northern Oman, Sol. Energy 206 (2020) 564–578, https://doi.org/10.1016/j.solener.2020.06.043.
[38] J. Atiq, P.K. Soori, Modelling of a grid connected solar PV system using MATLAB/simulink, Int. J. Simul. Syst. Sci. Technol. 17 (41) (2017) 45.1–4545, https://doi.org/10.5013/IJSSST.a.17.41.45.
[39] T. Suntio, T. Messo, Power electronics in renewable energy systems, Energies 12 (10) (2019), https://doi.org/10.3390/en12101852.
[40] M.H. De Freitas Takami, S.A. Oliveira Da Silva, L.P. Sampaio, Dynamic performance comparison involving grid-connected PV systems operating with active power-line conditioning and subjected to sudden solar irradiation changes, IET Renew. Power Gener. 13 (4) (2019) 587–597, https://doi.org/10.1049/iet-rpg.2018.5810.
[41] R. Errouissi, A. Al-Durra, S.M. Muyeen, A robust continuous-time MPC of a DC-DC boost converter interfaced with a grid-connected photovoltaic system, IEEE J. Photovoltaics 6 (6) (2016) 1619–1629, https://doi.org/10.1109/JPHOTOV.2016.2598271.
[42] A. Costa De Souza, F. Cardoso Melo, T. Lima Oliveira, C. Eduardo Tavares, Performance analysis of the computational implementation of a simplified PV model and MPPT algorithm, IEEE Lat. Am. Trans. 14 (2) (2016) 792–798, https://doi.org/10.1109/TLA.2016.7437224.
[43] M. Bajaj, A.K. Singh, Grid integrated renewable DG systems: a review of power quality challenges and state-of-the-art mitigation techniques, Int. J. Energy Res. 44 (1) (2020) 26–69, https://doi.org/10.1002/er.4847.
[44] T. Esram, P.L. Chapman, Comparison of photovoltaic array maximum power point tracking techniques, IEEE Trans. Energy Convers. 22 (2) (2007) 439–449, https://doi.org/10.1109/TEC.2006.874230.
[45] R.N. Kalaam, S.M. Muyeen, A. Al-Durra, H.M. Hasanien, K. Al-Wahedi, Optimisation of controller parameters for grid-tied photovoltaic system at faulty network using artificial neural network-based cuckoo search algorithm, Front. Cell Dev. Biol. 9 (2017) 1517–1526, https://doi.org/10.1049/iet-rpg.2017.0040.
[46] N. Cao, J. Liu, An improved maximum power point tracking for photovoltaic grid-connected inverter, 2013 IEEE Int. Conf. Mechatronics Autom. IEEE ICMA 2013 58 (1) (2013) 616–621, https://doi.org/10.1109/ICMA.2013.6617987.
[47] S. Prakash, S. Mishra, VSC control of grid connected PV for maintaining power supply during open-phase condition in distribution network, IEEE Trans. Ind. Appl. 55 (6) (2019) 6211–6222, https://doi.org/10.1109/TIA.2019.2932697.
[48] K. Prabha, Power System Stability and Control, 1994, p. 1176.
[49] R. Ntare, N.H. Abbasy, K.H.M. Youssef, Low voltage ride through control capability of a large grid connected PV system combining DC chopper and current limiting techniques, J. Power Energy Eng. 7 (1) (2019) 62–79, https://doi.org/10.4236/jpee.2019.71004.